Available online at www.sciencedirect.com

ScienceDirect

IFAC Papers Online CONFERENCE PAPER ARCHIVE

IFAC PapersOnLine 55-31 (2022) 497–504

Collision Avoidance for Underactuated Surface Vehicles in the Presence of Ocean Currents ⋆

Aurora Haraldsen * **Martin S. Wiig** ** **Kristin Y. Pettersen** *,**

* *Centre for Autonomous Marine Operations and Systems (NTNU AMOS), Department of Engineering Cybernetics, Norwegian University of Science and Technology, Trondheim, Norway (e-mail: {aurora.haraldsen, kristin.y.pettersen}@ntnu.no).*

** *Norwegian Defence Research Establishment (FFI), Kjeller, Norway. (e-mail: martin-syre.wiig@ffi.no).*

Abstract: This paper considers the problem of collision avoidance for surface vehicles moving under the influence of ocean currents. The vehicles we consider have underactuated dynamics, where the vehicle cannot directly control its lateral motion, which is a common trait of marine vehicles. We propose a reactive algorithm where the vehicle dynamics, including its underactuation and the effects of an ocean current disturbance, are handled directly in the avoidance strategy. Moreover, the algorithm only requires a limited amount of information about the obstacle and is proven to guarantee collision avoidance, as well as the completion of a nominal goal, under explicitly derived conditions. The theory is validated by simulations.

Keywords: collision avoidance, marine vehicles, underactuated dynamics, external disturbances

1. INTRODUCTION

Autonomous marine vehicles present a large potential for the future. During missions, it is essential that the vehicle is able to avoid collisions with unforeseen obstacles. This may be enabled by implementing a local navigation algorithm that takes over the control in emergency situations. However, even in nominal conditions, collision avoidance is not trivially achieved since marine vehicles generally lack control forces in the lateral direction. Moreover, unlike nonholonomic robots such as unicycles, marine vehicles will glide side-wise during turning maneuvers. In the presence of ocean currents, the control problem becomes even more challenging, as the current will directly affect the maneuverability of the vehicle, as well as present a kinematic bias influencing the vehicle velocity.

Reactive methods are important for handling unexpected events during missions, when a planning algorithm may be too slow, and can be used as the main navigation strategy in vehicles with too low computational power to perform planning. Existing approaches for reactive collision avoidance include the potential field method (Khatib, 1985), the dynamic window approach (Fox et al., 1997), the collision cone approach (Chakravarthy and Ghose, 1998), the constant avoidance angle algorithm (Wiig et al., 2020), velocity obstacles (Fiorini and Shiller, 1998), and control barrier functions (CBFs) (Ames et al., 2019). It is well-known that potential field methods have drawbacks with local minimima and oscillations as shown in Koren and Borenstein (1991). The dynamic window approach and CBFs are optimization-based and may therefore be too computationally heavy for the vehicle to perform. The remaining approaches are similar in that they are fundamentally based on the collision cone concept, which is both intuitive and computationally advantageous.

In this paper, we present a switching control algorithm that will enable an underactuated surface vehicle to complete its mission goal while avoiding collision with a dynamic obstacle, in the presence of ocean currents. The collision cone concept is used to generate safe references for the vehicle when a collision is imminent, which will temporarily take the vehicle away from its nominal objective. Although a similar concept has been applied to marine vehicles with underactuated dynamics in Wiig et al. (2020); Haraldsen et al. (2020), we here present an algorithm that also takes into account the effect of an ocean current disturbance, something which is rarely addressed in previous studies on marine collision avoidance. This is a significant lack, as ocean currents constitute a common disturbance which can significantly affect the vehicle maneuvers and overall stability. Therefore, we present a method that guarantees avoidance despite the additional difficulty of having an ocean current acting on the vehicle during its evasive maneuvers, under explicit conditions dependent on the strength of the current. Moreover, we show that a stronger current not only raises the requirement on the forward speed of the vehicle but also on its ability to change course, and we specifically consider these and similar effects in the design and underlying analysis of the algorithm. The theoretical results are validated by simulations.

The paper is organized as follows. The modeling of the marine vehicle and the ocean current disturbance is pre-

⋆ This work was supported by the Research Council of Norway through project No. 302435 and the Centres of Excellence funding scheme, project No. 223254 – NTNU AMOS.

10.1016/j.ifacol.2022.10.476

sented in Section 2. The control objectives are formulated in Section 3, and the obstacle modeling is presented in Section 4. The guidance algorithm that generates safe vehicle course directions is described in Section 5, and the control system that makes the vehicle keep the correct course is presented in Section 6. The overall system is analysed in Section 7, and simulations are provided in Section 8. Some concluding remarks are given in the last section.

2. CONTROL MODEL

We describe the horizontal motion of a marine vehicle using a maneuvering model (Fossen, 2011). We first state the model assumptions and present the modeling of the ocean current disturbance. Then we present the equations of motion in matrix-vector form, before giving the equations in component form.

2.1 Vehicle Assumptions

Assumption 1. The dynamics of the vehicle can be described in 3 degrees of freedom. That is, in the surge, sway, and yaw directions.

Assumption 2. The vehicle is port-starboard symmetric, and the origin of the body-fixed reference frame b is located at the center-line of the vehicle.

Assumption 3. The hydrodynamic damping is linear.

Remark 1. Hydrodynamic nonlinear damping is not included to reduce the model complexity, as the nonlinear damping terms are passive and should only enhance the directional stability of the craft.

Assumption 4. The origin of the body frame is located at the pivot point of the vehicle.

Remark 2. If the origin is not originally located at the pivot point, it is always possible to translate the origin to this point when the vessel is port-starboard symmetric (Fredriksen and Pettersen, 2004).

2.2 Ocean Current Disturbance

The effect of an ocean current is embodied in the vector

$$\boldsymbol{\nu}_{\mathrm{c}} \triangleq [u_{\mathrm{c}},\, v_{\mathrm{c}},\, r_{\mathrm{c}}]^T. \tag{1}$$

The state $\boldsymbol{\nu}_{\mathrm{c}}$ represents the velocity of the ocean current expressed in the vehicle-fixed reference frame b, where u_{c} and v_{c} are the velocities in the surge and sway directions and r_{c} is the angular rate. The ocean current directly impacts the velocity of the vehicle along these axes.

Assumption 5. The ocean current is known, and it is considered to be constant and irrotational with respect to the inertial reference frame, defined as $\boldsymbol{V}_{\mathrm{c}} \triangleq [V_x, V_y, 0]^T$. Moreover, there exists a positive constant $V_{\max}$ such that

$$\sqrt{V_x^2 + V_y^2} \leq V_{\max}. \tag{2}$$

Remark 3. Knowledge of $\boldsymbol{V}_{\mathrm{c}}$ can be obtained through an observer or directly from sensors such as an acoustic Doppler current profiler.

The ocean current in i is related to $\boldsymbol{\nu}_{\mathrm{c}}$ by the relation $\boldsymbol{\nu}_{\mathrm{c}} \triangleq \boldsymbol{R}^T(\psi_b)\boldsymbol{V}_{\mathrm{c}}$, where ψ_b is the orientation of the vehicle-fixed frame with respect to the inertial frame and

$$\boldsymbol{R}(\psi) \triangleq \begin{bmatrix} \cos(\psi) & -\sin(\psi) & 0 \\ \sin(\psi) & \cos(\psi) & 0 \\ 0 & 0 & 1 \end{bmatrix}. \tag{3}$$

2.3 Vehicle Equations of Motion

The state of the vehicle, $[\boldsymbol{\eta}_b^T,\, \boldsymbol{\nu}_b^T]^T$, describes the vehicle position and orientation and the linear and angular velocities. The position and orientation vector, $\boldsymbol{\eta}_b \triangleq [\boldsymbol{p}_b^T,\, \psi_b]^T$, is defined with respect to the inertial frame i, where $\boldsymbol{p}_b \triangleq [x_b,\, y_b]^T$. The body velocity vector, $\boldsymbol{\nu}_b \triangleq [u_b,\, v_b,\, r_b]^T$, is expressed in the body frame b, where u_b is the surge speed, v_b is the sway speed, and r_b is the yaw rate. In the presence of ocean currents, it is useful to express the velocity of the vehicle with respect to the current as $\boldsymbol{\nu}_r \triangleq \boldsymbol{\nu}_b - \boldsymbol{\nu}_c = [u_r,\, v_r,\, r_b]^T$. The vessel equations of motion then take the form (Fossen, 2011):

$$\dot{\boldsymbol{\eta}}_b = \boldsymbol{R}(\psi_b)\boldsymbol{\nu}_r + \boldsymbol{V}_{\mathrm{c}}, \tag{4a}$$

$$\boldsymbol{M}\dot{\boldsymbol{\nu}}_r + \boldsymbol{C}(\boldsymbol{\nu}_r)\boldsymbol{\nu}_r + \boldsymbol{D}\boldsymbol{\nu}_r = \boldsymbol{B}\boldsymbol{f}. \tag{4b}$$

It can be noticed that the ocean current acts as a kinematic bias in (4a) and consequently influences the linear vehicle velocity in i, $\boldsymbol{v}_b \triangleq \dot{\boldsymbol{p}}_b$, and thus the course of the vehicle, denoted as $\psi_f \triangleq \mathrm{atan2}(\dot{y}_b, \dot{x}_b)$. The matrix $\boldsymbol{M} = \boldsymbol{M}^T > 0$ represents the inertia and mass matrix, which includes hydrodynamic added mass. The matrix $\boldsymbol{D}$ accounts for hydrodynamic damping forces and satisfies $\boldsymbol{z}^T\boldsymbol{D}\boldsymbol{z} > 0, \forall \boldsymbol{z} \in \mathbb{R}^3 \backslash \{0\}$, and $\boldsymbol{C}(\boldsymbol{\nu}_r)$ is the Coriolis and centripetal matrix. The vector $\boldsymbol{f} \triangleq [T_u,\, \delta_r]^T$ contains the surge thrust T_u and the rudder angle δ_r, and $\boldsymbol{B} \in \mathbb{R}^{3\times 2}$ is the actuator configuration matrix which maps the control input vector to forces and moments acting on the body.

2.4 Vehicle Equations in Component Form

The equations of motion (4) may be expanded with respect to $\dot{\boldsymbol{\eta}}_b$ and $\dot{\boldsymbol{\nu}}_r$ as

$$\dot{x}_b = u_r\cos(\psi_b) - v_r\sin(\psi_b) + V_x, \tag{5a}$$

$$\dot{y}_b = u_r\sin(\psi_b) + v_r\cos(\psi_b) + V_y, \tag{5b}$$

$$\dot{\psi}_b = r_b, \tag{5c}$$

$$\dot{u}_r = F_u(u_r, v_r, r_b) + \tau_u, \tag{5d}$$

$$\dot{v}_r = F_v(u_r, v_r, r_b), \tag{5e}$$

$$\dot{r}_b = F_r(u_r, v_r, r_b) + \tau_r, \tag{5f}$$

where we have used that $\boldsymbol{M}^{-1}\boldsymbol{B}\boldsymbol{f} = [\tau_u, 0, \tau_r]^T$ under Assumption 4. Moreover, τ_u and τ_r are the control forces in surge and yaw, respectively, and the expressions of $F_u(\cdot)$, $F_v(\cdot)$, and $F_r(\cdot)$ are given in Appendix A. The sway dynamics (5e) can be further expanded as

$$\dot{v}_r = X(u_r)r_b + Y(u_r)v_r, \tag{6}$$

where $X(u_r)$ and $Y(u_r)$ are specified in Appendix A. We now state some assumptions regarding the dynamics (6).

Assumption 6. The term $X(u_r)$ satisfies

$$X(u_r) + u_r > 0, \quad \forall u_r > 0. \tag{7}$$

Assumption 7. The term $Y(u_r)$ satisfies

$$Y(u_r) < 0, \quad \forall u_r > 0. \tag{8}$$

Remark 4. Assumption 6 implies that a change in the orientation of the vehicle results in a change of its course, in nominal conditions without ocean currents. This property has been derived in e.g. Wiig et al. (2020) and is satisfied for most marine vehicles by design. Assumption 7 can be justified by contradiction; if $Y(u_r) > 0$ it would imply that the vehicle is nominally unstable in the sway direction. That is, a small perturbation would lead to the sway speed increasing indefinitely, which is clearly not feasible.

3. CONTROL OBJECTIVES

This section formalizes the control problem that is considered in this paper. The main objective is to make the marine vehicle avoid a collision with an obstacle of position $\boldsymbol{p}_o \triangleq [x_o,\, y_o]^T$. A second objective is proposed to demonstrate the flexibility of the collision avoidance algorithm. We call this the nominal objective, which represents the mission goal the vehicle should achieve. We propose to let the nominal objective of the vehicle be to follow a straight-line path $\mathcal{P} \triangleq \{(x,y) \in \mathbb{R}^2 \mid y = y_\mathrm{t}\}$, where y_t is the target position along the inertial y-axis, but note that the algorithm does not impose any restrictions on the nominal goal. The objectives are formalized as

$$d_{bo}(t) \geq d_{bo\,\min}, \qquad (9a) \qquad \lim_{t\to\infty} y_e(t) = 0, \qquad (9b)$$

where $y_e \triangleq y_b - y_\mathrm{t}$ is the cross-track error between the vehicle and the path, $d_{bo} \triangleq \|\boldsymbol{p}_b - \boldsymbol{p}_o\|$ is the distance to the obstacle, and $d_{bo\,\min} > 0$ is a minimum separation distance.

4. OBSTACLE MODEL

In this section, the model of the obstacle is stated, as well as the measurements that are needed to implement the algorithm presented in the next section.

The obstacle is modeled as the kinematic unicycle:

$$\dot{\boldsymbol{p}}_o = \boldsymbol{R}(\psi_o)\,[u_o\ 0]^T, \quad u_o \in [0, u_{o\,\max}], \qquad (10a)$$
$$\dot{\psi}_o = r_o, \quad r_o \in [-r_{o\,\max}, r_{o\,\max}], \qquad (10b)$$
$$\dot{u}_o = a_o, \quad a_o \in [-a_{o\,\max}, a_{o\,\max}], \qquad (10c)$$

where u_o is the forward speed and ψ_o is the heading angle. Moreover, a_o represents the linear acceleration and r_o the heading rate of the obstacle. Note that these are absolute values and thus the effect of the ocean current is implicitly included in the model. The kinematic equations (10) are a suitable representation that describe both moving and static objects, as well as a large class of vehicles. We assume that the minimum separation distance $d_{bo\,\min}$ is chosen large enough to account for the vehicle and obstacle areas such that they can be considered as moving points.

4.1 Required Measurements

An overview of the required measurements is shown in Figure 1, where the marine vehicle is given in blue and the obstacle in grey. The vehicle must be able to sense the distance to the obstacle, d_{bo}, which is used to decide when it must perform an evasive maneuver. To obtain a safe course direction for the maneuver, the vehicle must furthermore sense the collision cone of the obstacle, represented by the dashed lines in Figure 1. In general, a course direction in the interior of the cone will ultimately cause the vehicle to collide with the obstacle if it is static. The concept can be applied in the dynamic case by computing the course in a reference frame moving with the obstacle. Measurements of the velocity $\boldsymbol{v}_o \triangleq \dot{\boldsymbol{p}}_o$ must therefore be readily available in order to take into account the obstacle movements during the maneuver.

Remark 5. The distance to the obstacle and the collision cone can be measured using range sensors such as a lidars, radars, and sonars. Velocity measurements can be obtained from a Doppler radar or by using a tracking algorithm.

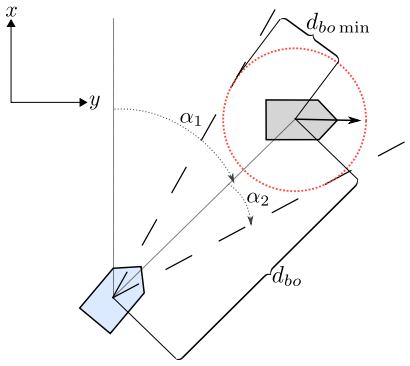

Fig. 1. Illustration of the measurements needed for the collision avoidance algorithm.

5. GUIDANCE ALGORITHM

In this section, we present the algorithm that computes the course direction the vehicle should keep in order to complete the objectives (9). Note that we choose to give the commanded angles as course references, as opposed to heading references, since the vehicle is capable of having a side-ways velocity that causes a deviation between the orientation of the vehicle and the cardinal direction it is moving in. This is both due to the ocean current and the vehicle's underlying dynamics. The structure of the algorithm is equal to that of Haraldsen et al. (2021b), which was inspired by Wiig et al. (2020), as it is not necessary to consider the ocean current explicitly at this stage. The ocean current will, however, have a significant impact on the analysis in Section 7, where conditions for choosing the design parameters of the algorithm are found.

5.1 Nominal Course Reference

The nominal course reference should make the vehicle converge to the desired path $\mathcal{P}$ by driving the cross-track error y_e to zero. To achieve this, the course angle is computed by a line-of-sight guidance law (Fossen, 2011):

$$\psi_{f\mathrm{nom}} \triangleq \operatorname{atan2}\left(-\frac{y_e}{\Delta}\right), \qquad (11)$$

where $\Delta > 0$ is a look-ahead distance, which was proven in Fossen and Pettersen (2014) to provide semi-global exponential convergence of the cross track error to zero when applied to vehicles such as the one modeled in (4a).

5.2 Safe Course Reference

The collision cone of the obstacle, $\mathcal{V} \triangleq (\psi_\nu^-, \psi_\nu^+)$, defines a set of unsafe vehicle course directions, where

$$\psi_\nu^\pm \triangleq \alpha_1 \pm \alpha_2. \qquad (12)$$

The angles α_1 and α_2 are found geometrically as

$$\alpha_1 \triangleq \operatorname{atan2}(y_o - y_b, x_o - x_b), \qquad (13)$$
$$\alpha_2 \triangleq \arcsin\left(\frac{d_{bo\,\min}}{d_{bo}}\right), \qquad (14)$$

as seen in Figure 1. The cone is rotated about the apex to account for changes in the position of the obstacle $\boldsymbol{p}_o$:

$$\psi_{\nu_o}^\pm \triangleq \psi_\nu^\pm + \psi_{v_o}^\pm, \qquad (15)$$

where the angles $\psi_{v_o}^\pm$ are defined as (Haraldsen et al., 2020)

$$\psi_{v_o}^\pm \triangleq \arcsin\left(\frac{u_o}{U_b}\sin\left(\pi - \psi_o + \psi_\nu^\pm\right)\right), \qquad (16)$$

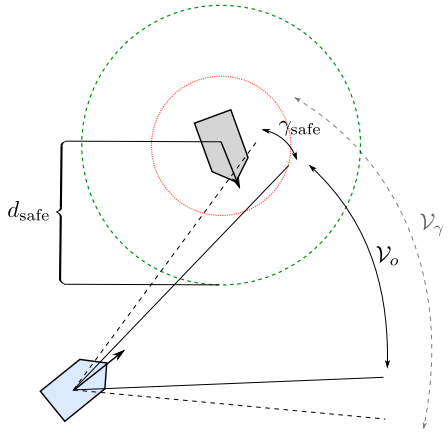

Fig. 2. Illustration of the collision avoidance scheme.

and we denote $U_b \triangleq \|\boldsymbol{v}_b\|$ the vehicle speed. To circumvent the obstacle safely, we let the safe course angles be defined in the exterior of $\mathcal{V}_o \triangleq \left(\psi^-_{\nu_o}, \psi^+_{\nu_o}\right)$ as

$$\psi^{\pm}_{f\text{ca}} = \psi^{\pm}_{\nu_o} \pm \gamma_{\text{safe}}, \tag{17}$$

where $\gamma_{\text{safe}} \in \left[0, \frac{\pi}{2}\right)$ is an additional avoidance angle which dictates how far the vehicle stays from the collision cone during the evasive maneuver.

5.3 Algorithm Definition

In order to choose the desired course direction of the vehicle, $\psi_{f\text{d}} \in \{\psi_{f\text{nom}}, \psi_{f\text{ca}}\}$, we define a safety distance $d_{\text{safe}} > d_{bo\,\min}$ around the obstacle, as illustrated in Figure 2. If, inside of this radius, the nominal course direction will lead to a collision, i.e. if

$$\begin{aligned} \psi_{f\text{nom}} &\in \mathcal{V}_\gamma \\ d_{bo} &\leq d_{\text{safe}} \end{aligned}, \tag{18}$$

then the desired course is chosen as $\psi_{f\text{d}} = \psi^j_{f\text{ca}}$ to make the vehicle diverge from the path and safely pass the obstacle, where $\mathcal{V}_\gamma$ is the set $\mathcal{V}_o$ extended by the angle γ_{safe} as shown in Figure 2. The evasive maneuver will be performed until it is safe for the vehicle to return to the path, i.e. until:

$$\psi_{f\text{nom}} \notin \mathcal{V}_\gamma, \tag{19}$$

at which point we let $\psi_{f\text{d}} = \psi_{f\text{nom}}$ once again. The parameter $j \in \{\pm\}$ determines the direction of the maneuver and signifies a clockwise and counter-clockwise turn. We let the direction be constant until a new maneuver is performed in accordance with (18) - (19). The parameter may be chosen to comply with the given sea regulations or possibly some other agreed upon set of rules. However, since we do not assume anything about the obstacle decision making, we here take a more conservative approach that will make the vehicle avoid a collision regardless of what the obstacle does, motivated by Wiig et al. (2020). Specifically, if the vehicle is on the boundary of the circle as the maneuver is initiated, that is $d_{bo} = d_{\text{safe}}$, we choose

$$j = \underset{j\in\{\pm\}}{\operatorname{argmax}} \left|\psi_o - \psi^j_{f\text{ca}}\right|. \tag{20}$$

This will make the vehicle attempt to maneuver behind the obstacle. If the vehicle is within the safe circle, we instead make it turn towards the closest safe candidate, i.e. we let

$$j = \underset{j\in\{\pm\}}{\operatorname{argmin}} \left|\psi_f - \psi^j_{f\text{ca}}\right|. \tag{21}$$

6. CONTROL SYSTEM

This section presents the control system that generates the control forces applied to the vehicle based on the course input received from the guidance algorithm. We here extend the control system of Haraldsen et al. (2021b) with the necessary modifications to compensate for the effects of an ocean current acting on the vehicle. This leads to a requirement on the vehicle relative surge speed, dependent on the strength of the ocean current, which enables the vehicle to control its course direction through the yaw angle and thus its accessible control forces.

6.1 Course Control

To make the vehicle track the commanded course angles, we define the desired course rate of the vehicle as

$$r_{f\text{d}} = \dot{\psi}_{f\text{d}} - k_\psi \tilde{\psi}_f, \tag{22}$$

where $\tilde{\psi}_f \triangleq \psi_f - \psi_{f\text{d}}$ is the course tracking error and $k_\psi > 0$ is the course control gain. It is straight-forward to verify that the above control law exponentially stabilizes the course error. However, due to the modular structure of the guidance algorithm, the assigned direction may be a discontinuous signal. In such cases, the vehicle will not be able to keep the required course rate temporarily due to actuator constraints. To be able to include this in the algorithm, we require that the following holds:

Assumption 8. The convergence time of the vehicle course rate, $r_f \triangleq \dot{\psi}_f$, to the desired rate, $r_{f\text{d}}$ (22), when the guidance algorithm switches from nominal guidance (11) to collision avoidance (17) is upper bounded by $T_{\text{switch}} > 0$.

6.2 Surge and Yaw Control

The achievement of the control objectives considered in this paper is not directly influenced by the vehicle surge speed. We therefore choose the desired relative speed as a constant, denoted by $u_{r\text{d}}(t) = U_{r\text{d}} > 0$, which provides some predictability for crossing vehicles and limits the wear and tear on the actuators. To maintain the maneuverability of the vehicle, the speed should exceed the strength of the ocean current and moreover meet the requirement:

Assumption 9. The desired relative surge speed satisfies

$$U_{r\text{d}} > \max\left\{V_{\max}, \frac{1}{2}V_{\max} - X_{\text{d}}\right\}. \tag{23}$$

We will control the course rate of the vehicle through the yaw control force. The course rate can be related to the yaw rate of the vehicle by the relationship

$$r_f = \frac{r_b\left(U^2_{b\text{d}} + X_{\text{d}}u_{b\text{d}} - u_{\text{c}}u_{b\text{d}} - v_{\text{c}}v_b\right) + v_r Y_{\text{d}} u_{b\text{d}}}{U^2_{b\text{d}}}, \tag{24}$$

which is found by differentiating $\psi_f = \psi_b + \operatorname{atan2}(v_b, u_{b\text{d}})$ under the assumption that $u_r \equiv U_{r\text{d}}$, and we introduce the notation $Y_{\text{d}} \triangleq Y(U_{r\text{d}})$, $X_{\text{d}} \triangleq X(U_{r\text{d}})$, $u_{b\text{d}} \triangleq U_{r\text{d}} + u_{\text{c}}$, and $U_{b\text{d}} \triangleq \sqrt{u^2_{b\text{d}} + v^2_b}$ for conciseness. In accordance with (24), we choose the desired yaw rate of the vehicle as

$$r_{b\text{d}} \triangleq \frac{U^2_{b\text{d}} r_{f\text{d}} - Y_{\text{d}} v_r u_{b\text{d}}}{U^2_{b\text{d}} + X_{\text{d}}u_{b\text{d}} - u_{\text{c}}u_{b\text{d}} - v_{\text{c}}v_b}. \tag{25}$$

To make the vehicle keep the desired speed and yaw rate, the following feedback linearizing controllers are applied:

$$\tau_u = -F_u(u_r, v_r, r_b) + \dot{u}_{r\text{d}} - k_u \tilde{u}_r, \tag{26a}$$

$$\tau_r = -F_r(u_r, v_r, r_b) + \dot{r}_{b\mathrm{d}} - k_r \tilde{r}_b, \tag{26b}$$

where $\tilde{u}_r \triangleq u_r - u_{r\mathrm{d}}$ is the surge speed error, $\tilde{r}_b \triangleq r_b - r_{b\mathrm{d}}$ is the yaw rate error, and $k_u, k_r > 0$ are the surge and yaw control gains. From (5) it is seen that the controllers (26) ensure global exponential tracking of the desired relative speed and yaw rate.

Assumption 10. At the time $t = t_0$, the vehicle has operated long enough for the yaw rate and surge speed to converge, that is $\tilde{u}_r(t_0) = \tilde{r}_b(t_0) = 0$.

Remark 6. The relation (24) is valid for all time $t \geq t_0$ under Assumption 10. Furthermore, to have a well-defined control input (26b), the denominator of (25) needs to be nonzero. We will show in Lemma 1 that this is implied under Assumptions 6 and 9.

7. CLOSED-LOOP ANALYSIS

We will in this section analyze the marine vehicle with the presented control system and guidance algorithm and arrive at a set of conditions ensuring vehicle safety and achievement of the nominal goal.

7.1 Lateral Speed Bound

During turning maneuvers, the vehicle will glide side-ways through the water by inducing a sway velocity relative to the ocean current. The overall speed of the vehicle is thus not only influenced by the ocean current but also the lateral vehicle motion through the relative sway speed v_r. In order to know how large the safety distance d_{safe} around the obstacle should be, it is necessary to have an upper bound of the vehicle speed. For this reason, we establish in the following lemma the conditions under which the lateral motion of the vehicle is bounded.

Lemma 1. Consider an underactuated marine vehicle modeled by (5). Let all stated assumptions hold, and suppose that the vehicle maintains a course rate, r_f, satisfying

$$|r_f(t)| \leq \kappa_{U_{r\mathrm{d}}} \frac{|Y_{\mathrm{d}}|}{|X_{\mathrm{d}}|} v_{r\max}, \quad \forall t \geq t_0, \tag{27}$$

where $\kappa_{U_{r\mathrm{d}}} \triangleq \frac{U_{r\mathrm{d}}}{U_{r\mathrm{d}} + V_{\max}}$. Then, if $|v_r(t_0)| \leq v_{r\max}$, the solutions of (5e) are bounded by

$$|v_r(t)| \leq v_{r\max}, \quad \forall t \geq t_0. \tag{28}$$

Proof. Consider the Lyapunov function candidate $V = \frac{1}{2} v_r^2$. The time-derivative of V along the system (5e) is

$$\dot{V} = \frac{U_{b\mathrm{d}}^2}{U_{b\mathrm{d}}^2 + X_{\mathrm{d}} u_{b\mathrm{d}} - u_{\mathrm{c}} u_{b\mathrm{d}} - v_{\mathrm{c}} v_b} \left(X_{\mathrm{d}} r_f v_r + Y_{\mathrm{d}} \left(1 - \frac{u_{\mathrm{c}} u_{b\mathrm{d}} + v_{\mathrm{c}} v_b}{U_{b\mathrm{d}}^2} \right) v_r^2 \right), \tag{29}$$

where we have used the relations (6) and (24). To ensure that the quadratic term is negative definite, we require

$$\begin{aligned} &U_{b\mathrm{d}}^2 - u_{\mathrm{c}} u_{b\mathrm{d}} - v_{\mathrm{c}} v_b = \\ &U_{r\mathrm{d}}^2 + U_{r\mathrm{d}} \|\boldsymbol{V}_{\mathrm{c}}\| \cos(\chi_{\mathrm{c}}) + v_r^2 + v_r \|\boldsymbol{V}_{\mathrm{c}}\| \sin(\chi_{\mathrm{c}}) > 0. \end{aligned} \tag{30}$$

In the last line, u_{c} and v_{c} are given in amplitude-phase form, where $\chi_{\mathrm{c}} \triangleq \mathrm{atan2}\,(v_{\mathrm{c}}, u_{\mathrm{c}})$. Using that

$$\min_{v_r} \left\{ v_r^2 + v_r \|\boldsymbol{V}_{\mathrm{c}}\| \sin(\chi_{\mathrm{c}}) \right\} = -\frac{\|\boldsymbol{V}_{\mathrm{c}}\|^2 \sin^2(\chi_{\mathrm{c}})}{4}, \tag{31}$$

minimizing (30) with respect to χ_{c} gives

$$U_{b\mathrm{d}}^2 - u_{\mathrm{c}} u_{b\mathrm{d}} - v_{\mathrm{c}} v_b \geq U_{r\mathrm{d}} (U_{r\mathrm{d}} - V_{\max}) > 0, \tag{32}$$

where we have used Assumptions 5, 6, and 9. It follows

$$1 - \frac{u_{\mathrm{c}} u_{b\mathrm{d}} + v_{\mathrm{c}} v_b}{U_{b\mathrm{d}}^2} \geq \kappa_{U_{r\mathrm{d}}}. \tag{33}$$

Similar arguments can be used to show that

$$U_{b\mathrm{d}}^2 + X_{\mathrm{d}} u_{b\mathrm{d}} - u_{\mathrm{c}} u_{b\mathrm{d}} - v_{\mathrm{c}} v_b \geq \kappa_{X_{\mathrm{d}}} > 0, \tag{34}$$

where $\kappa_{X_{\mathrm{d}}} \triangleq (U_{r\mathrm{d}} - V_{\max})(U_{r\mathrm{d}} + X_{\mathrm{d}})$, which verifies that (25) is well-defined. It follows from Assumption 7 that

$$\dot{V} \leq \frac{U_{b\mathrm{d}}^2}{\kappa_{X_{\mathrm{d}}}} \left(|X_{\mathrm{d}}|\, |r_f| |v_r| - \kappa_{U_{r\mathrm{d}}} |Y_{\mathrm{d}}|\, v_r^2 \right). \tag{35}$$

The rest of the proof follows the reasoning presented in Wiig et al. (2017, Lemma 1). Define the level set $\Omega_{v_r} \triangleq \{ v_r \in \mathbb{R} \mid V \leq \frac{1}{2} v_{r\max}^2 \}$. Condition (27) with (35) ensures that $\dot{V} \leq 0$ on the boundary of this set. Thus, Ω_{v_r} is a positively invariant set, and any trajectory $v_r(t)$ starting inside of it cannot leave it.

7.2 Guaranteed Collision Avoidance

To ensure that the condition (27) is fulfilled and hence that the speed of vehicle is bounded, we require that

Assumption 11. The desired course rate (22) is saturated such that $r_{f\mathrm{d}} \in [-r_{f\max}, r_{f\max}]$, where

$$r_{f\max} \triangleq \kappa_{U_{r\mathrm{d}}} \frac{|Y_{\mathrm{d}}|}{|X_{\mathrm{d}}|} v_{r\max}. \tag{36}$$

Since the course reference $\psi_{f\mathrm{d}}$ can be discontinuous, Assumption 11 also prevents the desired course rate from becoming overly large during steps. The next lemma derives the conditions that enable us to choose the parameter (36) to guarantee collision avoidance under the proposed control scheme.

Lemma 2. Consider an underactuated marine vehicle modeled by (5) and an obstacle modeled by (10). Let all stated assumptions hold. Suppose the vehicle maintains a relative surge speed $u_r(t) = U_{r\mathrm{d}}$, $\forall t \geq t_0$, satisfying

$$b - \sqrt{4ac} > 0, \tag{37}$$

where the constants a, b, and c will be defined in the proof of this lemma, and a course rate satisfying $r_f(t) = r_{f\mathrm{d}}(t)$, $\forall t \geq t_1$, where $t_1 \geq t_0$. Furthermore, let $\psi_{f\mathrm{d}}(t) = \psi_{f\mathrm{ca}}^j(t)$, $\forall t \geq t_1$, and suppose that there exists a time $t_2 \geq t_1$ at which the parameter j satisfies (21) and

$$\psi_f(t_2) \notin \mathcal{V}_o(t_2). \tag{38}$$

Then, if $|v_r(t_0)| \leq v_{r\max}$, where the maximum sway speed is chosen in the interval $v_{r\max} \in [v_{r\max}^-, v_{r\max}^+]$, with

$$v_{r\max}^{\pm} \triangleq \frac{-b \pm \sqrt{b^2 - 4ac}}{2a}, \tag{39}$$

a collision will not occur for the remaining time, that is

$$d_{bo}(t) \geq d_{bo\min}, \quad \forall t \geq t_2. \tag{40}$$

Proof. We will first prove that by staying on a course in the exterior of the collision cone, the vehicle will avoid a collision with the obstacle. Let $\psi_{fo} \triangleq \mathrm{atan2}(\dot{y}_b - \dot{y}_o, \dot{x}_b - \dot{x}_o)$ denote the relative course direction of the vehicle with respect to the obstacle. We consider relative terms as this

simplifies the analysis. It is seen geometrically that the condition (38) is equivalent to

$$|\psi_{fo}(t_2) - \alpha_1(t_2)| \geq \alpha_2(t_2), \tag{41}$$

which can be verified trivially. The rest follows the similar arguments as in (Haraldsen et al., 2021a, Lemma 1). The time-derivative of the distance, d_{bo}, is found geometrically:

$$\dot{d}_{bo} = -U_{bo}\cos(\psi_{fo} - \alpha_1), \tag{42}$$

where $U_{bo} \triangleq \|\boldsymbol{v}_b - \boldsymbol{v}_o\|$. Assuming the inequality (41) holds for all $t \geq t_2$ and substituting the expression for α_2 (14), the solutions of (42) satisfy

$$d_{bo}(t) \geq d_{bo\,\min}, \quad \forall t \geq t_2, \tag{43}$$

which concludes this part of the proof.

To stay on a safe course, the course rate of the vehicle must exceed the rate of change of obstacle collision cone. As a minimum, this must hold for the case $\psi_f = \psi^j_{\nu_o}$, which implies that the course of the vehicle is on the boundary of the collision cone set. The time-derivative of $\psi^j_{\nu_o}$ (15) is

$$\dot{\psi}^{\pm}_{\nu_o} = \dot{\psi}^{\pm}_{\nu} + \dot{\psi}^{\pm}_{v_o}. \tag{44}$$

where

$$\begin{aligned}\dot{\psi}^{\pm}_{v_o} = \left(r_o - \dot{\psi}^{\pm}_{\nu}\right) P\left(\vartheta^{\pm}\right) + a_o Q\left(\vartheta^{\pm}\right) \\ - \left(v_b \dot{v}_b + u_b \dot{u}_b\right) R\left(\vartheta^{\pm}\right),\end{aligned} \tag{45}$$

by (16), with $\vartheta^{\pm} \triangleq \pi - \psi_o + \psi^{\pm}_{\nu}$ and

$$P\left(\vartheta^{\pm}\right) \triangleq \frac{u_o \cos\left(\vartheta^{\pm}\right)}{\sqrt{U_{bd}^2 - u_o^2 \sin^2\left(\vartheta^{\pm}\right)}}, \tag{46a}$$

$$Q\left(\vartheta^{\pm}\right) \triangleq \frac{\sin\left(\vartheta^{\pm}\right)}{\sqrt{U_{bd}^2 - u_o^2 \sin^2\left(\vartheta^{\pm}\right)}}, \tag{46b}$$

$$R\left(\vartheta^{\pm}\right) \triangleq \frac{u_o \sin\left(\vartheta^{\pm}\right)}{U_{bd}^2\sqrt{U_{bd}^2 - u_o^2 \sin^2\left(\vartheta^{\pm}\right)}}. \tag{46c}$$

The time-derivative of ψ^j_{ν} (12) is

$$\dot{\psi}^{\pm}_{\nu} = -\frac{U_{bo}}{d_{bo}}\left(\sin(\psi_{fo} - \alpha_1) \mp \cos(\psi_{fo} - \alpha_1)\tan(\alpha_2)\right). \tag{47}$$

Since $\psi_f = \psi^{\pm}_{\nu_o} \implies \psi_{fo} - \alpha_1 = \pm\alpha_2$, we have

$$\dot{\psi}^{\pm}_{\nu} = \frac{U_{bo}}{d_{bo}}\left(\mp\sin(\alpha_2) \pm \cos(\alpha_2)\tan(\alpha_2)\right) = 0. \tag{48}$$

Inserting $\dot{u}_c = r_b v_c$ and $\dot{v}_c = -r_b u_c$ gives

$$\begin{aligned}\dot{\psi}^{\pm}_{\nu_o} = r_o P\left(\vartheta^{\pm}\right) + a_o Q\left(\vartheta^{\pm}\right) \\ - \left(r_b\left(X_d v_b - v_b u_c + u_{bd} v_c\right) + Y_d v_b v_r\right) R\left(\vartheta^{\pm}\right).\end{aligned} \tag{49}$$

Then, substituting $r_f = \pm\dot{\psi}^{\pm}_{\nu_o}$ and the relation (24) for r_b, we obtain a closed expression for $\dot{\psi}^{\pm}_{\nu_o}$ as

$$\dot{\psi}^{\pm}_{\nu_o} = \frac{G_n}{G_d}, \tag{50}$$

where

$$\begin{aligned}G_n \triangleq r_o P\left(\vartheta^{\pm}\right) + a_o Q\left(\vartheta^{\pm}\right) \\ + \frac{U_{bd}^2 Y_d v_r^2 R\left(\vartheta^{\pm}\right)}{U_{bd}^2 + X_d u_{bd} - u_c u_{bd} - v_c v_b},\end{aligned} \tag{51}$$

$$G_d \triangleq 1 \pm R\left(\vartheta^{\pm}\right)\frac{U_{bd}^2\left(X_d v_b - v_r u_c + U_{rd} v_c\right)}{U_{bd}^2 + X_d u_{bd} - u_c u_{bd} - v_c v_b}. \tag{52}$$

Using Assumptions 5, 6, and 9, an upper bound $\left|\dot{\psi}^{\pm}_{\nu_o}\right| \leq \frac{G_{n\,\max}}{G_{d\,\min}} \coloneqq F_{\nu_o}$ can be found, where

$$\begin{aligned}G_{n\,\max} \triangleq \frac{v_r^2\,|Y_d|\,u_{o\,\max}}{\kappa_{X_d}\sqrt{(U_{rd} - V_{\max})^2 - u_{o\,\max}^2}} \\ + \frac{a_{o,\max}}{\sqrt{(U_{rd} - V_{\max})^2 - u_{o\,\max}^2}} + r_{o\,\max}\frac{u_{o\,\max}}{U_{rd} - V_{\max}},\end{aligned} \tag{53}$$

$$G_{d\,\min} \triangleq 1 - u_{o\,\max}\frac{|X_d||v_r| + V_{\max}}{\kappa_{X_d}\sqrt{(U_{rd} - V_{\max})^2 - u_{o\,\max}^2}}. \tag{54}$$

Hence, in the worst case scenario, we must have

$$\kappa_{U_{rd}}\frac{|Y_d|}{|X_d|}v_{r\,\max} \geq F_{\nu_o}(v_{r\,\max}). \tag{55}$$

in order to comply with Assumption 11. The inequality (55) has the solution $v_{r\,\max} \in [v^-_{r\,\max}, v^+_{r\,\max}]$ if and only if $b > 0$ and $b \geq \sqrt{4ac}$, where

$$a \triangleq -|Y_d|u_{o\,\max}\frac{\kappa_{U_{rd}} + 1}{\kappa_{X_d}\sqrt{(U_{rd} - V_{\max})^2 - u_{o\,\max}^2}}, \tag{56}$$

$$b \triangleq \frac{|Y_d|}{|X_d|}\left(\kappa_{U_{rd}} - \frac{\kappa_{U_{rd}} u_{o\,\max} V_{\max}}{\kappa_{X_d}\sqrt{(U_{rd} - V_{\max})^2 - u_{o\,\max}^2}}\right), \tag{57}$$

$$c \triangleq -\frac{r_{o\,\max}u_{o\,\max}}{U_{rd} - V_{\max}} - \frac{a_{o,\max}}{\sqrt{(U_{rd} - V_{\max})^2 - u_{o\,\max}^2}}. \tag{58}$$

Hence, it follows from (37) that the vehicle will maintain a safe course and avoid a collision for all time $t \geq t_2$.

Remark 7. Similar to the proof of Haraldsen et al. (2021b, Lemma 3), we show in Lemma 2 that the vehicle will avoid a collision with the obstacle as long as it is able to remain on a safe course direction. For vehicles with underactuated sway dynamics, this is not trivially achieved due to the coupling between the course rate of the vehicle and its swaying motion. Notice also that in the case of a weak or insignificant ocean current $V_{\max} \approx 0$, the avoidance requirement (55) reduces exactly to the one found in Haraldsen et al. (2021b), where ocean currents were not considered. It is shown here that the effect of an ocean current places higher requirements on the vehicle course rate and relative surge speed in order to guarantee avoidance.

7.3 Safe Path Following in the Presence of Ocean Currents

We will combine the previous results to derive the main theorem, which states the complete set of conditions under which the proposed algorithm enables the underactuated vehicle to converge to the desired path without a collision, while moving under the influence of ocean currents. For brevity, we introduce the parameters $U_{r\,\max} \triangleq \sqrt{U_{rd}^2 + v_{r\,\max}^2}$ and $U_{b\,\max} \triangleq \sqrt{U_{r\,\max}^2 + V_{\max}^2 + 2V_{\max}U_{r\,\max}}$.

Theorem 1. Consider an obstacle modeled as (10). Let all stated assumptions hold, conditions (37) and (39) of Lemma 2 hold, and, for some $\epsilon \in (0, \pi]$, the look-ahead distance satisfy

$$\Delta \geq \frac{|X_d|\,U_{b\,\max}}{\kappa_{U_{rd}}\,|Y_d|\,v_{r\,\max} - \epsilon\,|X_d|\,k_\psi}. \tag{59}$$

Furthermore, let the additional avoidance angle satisfy

$$\gamma_{\text{safe}} \geq \arccos\left(\frac{d_{bo\,\min}}{d_{bo\,\min} + T_{\text{switch}}(U_{b\,\max} + u_{o\,\max})}\right), \tag{60}$$

and the safety distance satisfy

$$d_{\text{safe}} \geq d_o + d_{\text{turn}} + U_{b\,\max}T_{\text{switch}} + d_{bo\,\min}, \tag{61}$$

where

$$d_{\text{turn}} \triangleq \frac{U_{b\max}}{\min\left\{r_{f\max}, \frac{k_\psi}{\text{Si}\left(\frac{\pi}{2}\right)}\right\}}, \tag{62}$$

$$t_{\text{turn}} \triangleq \max\left\{\frac{\pi}{r_{f\max}}, \frac{\ln\left(\frac{\pi}{\gamma_{\text{safe}}}\right)}{k_\psi}\right\}, \tag{63}$$

and $d_o \triangleq u_{o\max}(t_{\text{turn}} + T_{\text{switch}})$. Then, if $|v_r(t_0)| \leq v_{r\max}$ and $d_{bo}(t_0) \geq d_{\text{safe}}$, the underactuated marine vehicle modeled by (5) and controlled by the surge and yaw controllers (26a)-(26b), the course controller (22), the guidance law (11), and the collision avoidance algorithm (17)-(21), will achieve the control objectives (9) and maintain a bounded sway speed $|v_r(t)| \leq v_{r\max}$ for all $t \geq t_0$.

Proof. It follows from Assumption 11 and Lemma 1 that the relative sway speed is bounded by $|v_r| \leq v_{r\max}$. Hence, by Assumption 5, $U_b \leq U_{b\max}$.

Suppose the vehicle must avoid a collision by (18) as the distance d_{bo} equals d_{safe}. Over the time T_{switch}, the vehicle will reach the required rate r_{fd}. In the worst case scenario, the vehicle travels directly towards the obstacle at a speed of $U_{b\max}$. Then, the vehicle will proceed to turn towards the angle ψ^j_{fca}. The turn cannot be larger than π rad by definition. It follows from (22) that the convergence time from $|\tilde{\psi}_f| = \pi$ to $|\tilde{\psi}_f| \leq \gamma_{\text{safe}}$ is $t_{\text{turn}} = \frac{\ln\left(\frac{\pi}{\gamma_{\text{safe}}}\right)}{k_\psi}$. The vehicle will then have reached the exterior of the collision cone. The distance traveled by the vehicle towards the obstacle over this turn is $d_{\text{turn}} = \frac{U_{b\max}}{k_\psi}\text{Si}\left(\frac{\pi}{2}\right)$ (Wiig et al., 2017, Lemma 3). However, if $|r_{fd}| \geq r_{f\max}$, we alternatively have $t_{\text{turn}} = \frac{\pi}{r_{f\max}}$ and $d_{\text{turn}} = \frac{U_{b\max}}{r_{f\max}}$. The distance traveled by the obstacle towards the vehicle can at most be d_o over this maneuver. Hence, there exists a time at which all conditions of Lemma 2 are satisfied before the distance d_{bo} is reduced to less than $d_{bo\min}$. Similarly, if a maneuver is initiated while $d_{bo} < d_{\text{safe}}$, it follows from the avoidance angle γ_{safe} (60) that the vehicle maintains a course in the exterior of the collision cone until $r_f = r_{fd}$ and Lemma 2 can be applied (Haraldsen et al., 2021b, Theorem 1). Since the vehicle maintains a relative surge speed satisfying (37), which implies that $U_{\text{rd}} - V_{\max} > u_{o\max}$, there exists a time at which the vehicle has fully escaped the obstacle and satisfies $\psi_{fd} = \psi_{f\text{nom}}$ for all future time. An upper bound $|\dot{\psi}_{f\text{nom}}| \leq \frac{U_{\text{bd}\max}}{\Delta}$ is found from (11), which combined with (36) and (59) shows that $r_{f\max} > |\dot{\psi}_{f\text{nom}}|$. Hence, the vehicle will eventually reach $|\tilde{\psi}_f| \leq \epsilon$, from which it satisfies the control law (22) by the choice of Δ (59). It follows that the vehicle reaches the desired path $\mathcal{P}$ and stays on it thereafter.

8. SIMULATION RESULTS

This section presents a simulation of the proposed control algorithm applied to a light AUV (LAUV). In the simulation, the LAUV moves in the horizontal plane, thus satisfying the model (4). The numerical parameters of the vehicle are found in Estrela da Silva et al. (2007). The remaining parameters used in the simulation are as follows:

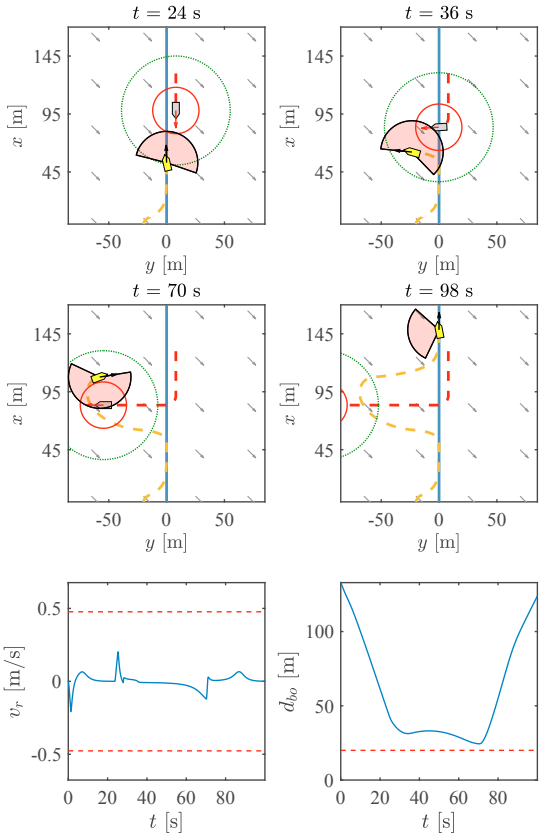

Fig. 3. North-East (NE) plots of the simulation results, and the relative vehicle sway speed v_r and distance d_{bo} plotted with respect to time. The NE plots shows the vehicle in yellow and the obstacle in grey. The distances $d_{bo\min}$ and d_{safe} are demonstrated by the red and green circles, respectively. The cone $\mathcal{V}_\gamma$ is shown as the red, transparent sector and the path $\mathcal{P}$ as the blue line. The vehicle and obstacle trajectories are represented by the yellow and red dashed lines.

$r_{o\max} = 0.2$ rad/s	$V_x = -0.6$ m/s	$V_y = 0.6$ m/s
$a_{o\max} = 0.05$ m/s^2	$U_{\text{rd}} = 3$ m/s	$k_\psi = 0.5$ s^{-2}
$u_{o\max} = 1.6$ m/s	$\epsilon = \frac{\pi}{6}$ rad	$k_r = 1$ s^{-1}
$v_{r\max} = 0.48$ m/s	$\Delta = 6$ m	$k_u = 1$ s^{-1}
$r_{f\max} = 0.96$ rad/s	$d_{bo\min} = 20$ m	$d_{\text{safe}} = 47$ m
$T_{\text{switch}} = 1.92$ s	$y_{\text{t}} = 0$ m	$\gamma_{\text{safe}} = 0.86$ rad

All design parameters were chosen to satisfy the assumptions of Theorem 1, which can be verified trivially. Moreover, $Y_{\text{d}} = -3.7857$ and $X_{\text{d}} = -1.4514$, which fulfills Assumptions 6 and 7. The results of the simulation can be seen in Figure 3. The obstacle moves with increasing speed along the vehicle path, which requires the vehicle to diverge from the path in accordance with condition (18). The obstacle proceeds to take a right turn simultaneously as the vehicle passes on the right side. The vehicle is then required to move further aside to avoid a collision. From Figure 3 it is seen that the algorithm takes the vehicle safely past the obstacle despite a significant ocean current acting on it, and the vehicle converges to the path once it has evaded the obstacle. Moreover, the relative sway speed remains within the defined bounds, which supports the result of Theorem 1.

9. CONCLUSIONS

In this paper, we have presented the development and analysis of a reactive collision avoidance algorithm that will enable an underactuated surface vehicle moving under the influence of ocean currents to avoid a collision with an obstacle and moreover achieve its overall goal. The algorithm is based on defining a safe circle around the obstacle, in which the vehicle must maintain safe course directions and thus temporarily diverge from its nominal behaviour if necessary. Safe directions are defined using the collision cone of the obstacle, and we make the vehicle keep an additional avoidance angle to the collision cone to take into account discontinuities in the assigned course directions caused by the modular nature of the algorithm. The proposed method guarantees that the vehicle avoids a collision with the obstacle if the derived avoidance criteria are fulfilled, shown by a rigorous analysis of the closed-loop system. The analysis generalizes previous results on the similar concept with the additional complexity of having an constant and irrotational ocean current acting on the vehicle. This leads to stricter requirements on the vehicle relative surge speed and course rate in order to guarantee collision avoidance, dependent on the strength of the ocean current. The safety distance and avoidance angle are similarly enhanced to account for a potentially higher absolute speed of the vehicle when moving in ocean currents. Simulations are provided to demonstrate the algorithm and validate the analysis.

REFERENCES

Ames, A.D., Coogan, S., Egerstedt, M., Notomista, G., Sreenath, K., and Tabuada, P. (2019). Control barrier functions: Theory and applications. In *Proc. 2019 18th European Control Conference*, 3420–3431.

Chakravarthy, A. and Ghose, D. (1998). Obstacle avoidance in a dynamic environment: a collision cone approach. *IEEE Trans. on Systems, Man, and Cybernetics - Part A: Systems and Humans*, 28(5), 562–574.

Estrela da Silva, J., Terra, B., Martins, R., and Sousa, J. (2007). Modeling and simulation of the LAUV autonomous underwater vehicle. In *Proc. IEEE IFAC Int. Conf. on Methods and Models in Automation and Robotics*.

Fiorini, P. and Shiller, Z. (1998). Motion planning in dynamic environments using velocity obstacles. *The Int. Journal of Robotics Research*, 17(7), 760–772.

Fossen, T.I. (2011). *Handbook of Marine Craft Hydrodynamics and Motion Control*. John Wiley & Sons.

Fossen, T.I. and Pettersen, K.Y. (2014). On uniform semiglobal exponential stability (USGES) of proportional line-of-sight guidance laws. *Automatica*, 50(11), 2912–2917.

Fox, D., Burgard, W., and Thrun, S. (1997). The dynamic window approach to collision avoidance. *IEEE Robotics Automation Magazine*, 4(1), 23–33.

Fredriksen, E. and Pettersen, K. (2004). Global κ-exponential way-point manoeuvering of ships. In *Proc. 43rd IEEE Conf. on Decision and Control*, 5360–5367.

Haraldsen, A., Wiig, M.S., and Pettersen, K.Y. (2020). Vehicle safety of the velocity obstacle algorithm. In *Proc. 2020 59th IEEE Conf. on Decision and Control*, 5340–5347.

Haraldsen, A., Wiig, M.S., and Pettersen, K.Y. (2021a). Reactive collision avoidance for nonholonomic vehicles in dynamic environments with obstacles of arbitrary shape. *IFAC-PapersOnLine*, 54(14), 155–160. Proc. 3rd IFAC Conf. on Modelling, Identification and Control of Nonlinear Systems.

Haraldsen, A., Wiig, M.S., and Pettersen, K.Y. (2021b). Reactive collision avoidance for underactuated surface vehicles using the collision cone concept. In *Proc. IEEE Conf. on Control Technology and Applications*, 619–626.

Khatib, O. (1985). Real-time obstacle avoidance for manipulators and mobile robots. In *Proc. IEEE Int. Conf. on Robotics and Automation*, 500–505.

Koren, Y. and Borenstein, J. (1991). Potential field methods and their inherent limitations for mobile robot navigation. In *Proc. IEEE Int. Conf. on Robotics and Automation*, 1398–1404.

Wiig, M.S., Pettersen, K.Y., and Krogstad, T.R. (2020). Collision avoidance for underactuated marine vehicles using the constant avoidance angle algorithm. *IEEE Trans. on Control Systems Technology*, 28(3), 951–966.

Wiig, M.S., Pettersen, K.Y., and Krogstad, T.R. (2017). A reactive collision avoidance algorithm for vehicles with underactuated dynamics. In *Proc. 56th IEEE Conf. Decision and Control*, 1452–1459.

Appendix A. FUNCTIONAL EXPRESSIONS

The functional expressions of the model (5) are

$$F_u(u_r, v_r, r_b) \triangleq r_b \frac{r_b m_{23} + v_r m_{22}}{m_{11}} - u_r \frac{d_{11}}{m_{11}}, \tag{A.1}$$

$$F_r(u_r, v_r, r_b) \triangleq r_b \frac{m_{23}\left(d_{23} - m_{11}u_r\right) - m_{22}\left(d_{33} + m_{23}u_r\right)}{m_{22}m_{33} - m_{23}^2} + v_r \frac{m_{23}d_{22} + m_{22}\left(d_{32} + u_r\left(m_{22} - m_{11}\right)\right)}{m_{22}m_{33} - m_{23}^2}, \tag{A.2}$$

$$F_v(u_r, v_r, r_b) \triangleq \underbrace{r_b \frac{d_{33}m_{23} - d_{23}m_{33} + u_r\left(m_{23}^2 - m_{11}m_{33}\right)}{m_{22}m_{33} - m_{23}^2}}_{X(u_r)} + \underbrace{v_r \frac{d_{32}m_{23} - d_{22}m_{33} + u_r m_{23}\left(m_{22} - m_{11}\right)}{m_{22}m_{33} - m_{23}^2}}_{Y(u_r)}, \tag{A.3}$$

where m_{ij} and d_{ij} are the elements of the inertia matrix $\boldsymbol{M}$ and damping matrix $\boldsymbol{D}$, respectively.